A Kinetic Model for Precipitation of TiN Inclusions From Both Homogeneous and Heterogeneous Nucleation During Solidification of Steel

QIFENG SHU, VILLE-VALTTERI VISURI, TUOMAS ALATARVAS, and TIMO FABRITIUS

Complex TiN + oxide inclusions which nucleate and grow on the surface of the primary oxide inclusions, *e.g.* MgO, have been frequently observed in various steel grades after solidification. To describe the precipitation kinetics of TiN and TiN + MgO inclusions, a model accounting for both heterogeneous and homogeneous nucleation was proposed in this work. The model was validated by employing the literature data, and good agreement has been achieved between experimental data and calculation data. The influence of nitrogen and titanium concentrations, the interfacial tension between TiN and steel, cooling rate, and size distribution of primary oxides on the size distribution of TiN and TiN + MgO inclusions were investigated by the model calculations. It was found that nitrogen and titanium concentrations, the interfacial tension between TiN and steel, and the number density of primary MgO inclusions have an impact on the final size distributions of TiN and TiN + MgO inclusions. In contrast, the effects of cooling rate and size of MgO inclusions on the final inclusion size distribution are negligible. The large interfacial tension between TiN and steel would suppress the homogeneous nucleation and is favorable to heterogeneous nucleation. The increase of the number density of primary MgO can significantly suppress the homogeneous nucleation and reduce the size of TiN + MgO inclusions. The present model can be extended to describe the heterogeneous precipitation of other complex inclusions providing that the secondary inclusion has a low lattice mismatch with the primary inclusion. Combining the present model with our previous model for the size distribution of primary inclusions, the size distribution of inclusions in solidified steel can be well described and controlled.

I. INTRODUCTION

NON-METALLIC inclusions affect the mechanical properties and lifespan of final products.[1] Generally, non-metallic inclusions are detrimental to the strength, ductility, and fatigue properties of steel and could lead to the cracking and pitting corrosion of steel. For example, large titanium nitride inclusions deteriorate the fatigue properties of bearing steels.[2] The susceptibility to hydrogen-induced cracking in steels can be enhanced by elongated manganese sulfide inclusions.[3] On the other hand, non-metallic inclusions, especially small ones can act as the heterogeneous nucleation sites for precipitations of fine acicular ferrites and increase the strength of steel, which is known as "oxide metallurgy".[4]

The endogenous inclusions are originated from both the deoxidation/reoxidation of steel and segregation during the solidification of steel. The majority of endogenous inclusions are formed by deoxidation and reoxidation during steel refining and continuous casting and these inclusions can be termed "primary inclusions".[5] Some oxide, sulfide and nitride inclusions, also known as "secondary inclusions", can be precipitated from steel during solidification due to the supersaturation of segregated elements in the inter-dendritic area.[6,7] These inclusions can be harmful to the steel properties, but small ones can be employed as the nucleation sites of fine steel structures. All these effects on steel properties are determined by the composition and size distribution of inclusions.

QIFENG SHU, VILLE-VALTTERI VISURI, TUOMAS ALATARVAS, and TIMO FABRITIUS are with the Process Metallurgy Research Unit, University of Oulu, Oulu 90014, Finland. Contact e-mail: qifenq.shu@oulu.fi; shuqifeng@gmail.com

Some complex inclusions are frequently observed in steels after solidification. In ingots after electro slag remelting, complex inclusions with precipitated TiN on the core of the spinel are often found.[8] These complex spinel + TiN inclusions are also observed in bearing steels.[9] Pervushin and Suito[10] found that TiN can nucleate on the particles of Al_2O_3, ZrO_2, Ce_2O_3 and MgO. The number of particles per area for TiN + MgO was larger than those of TiN precipitated on Al_2O_3, ZrO_2 and Ce_2O_3, while the mean diameter of TiN + MgO was smaller than those of TiN precipitated on other particles. In advanced high strength steel with high manganese content, manganese sulfides were found to be precipitated on Al_2O_3 and AlN to form complex Al_2O_3-MnS and AlN-MnS inclusions.[11] The formation of these complex inclusions indicates that heterogeneous nucleation of secondary inclusions, e.g. TiN and MnS on primary inclusions ($MgAl_2O_4$, MgO, …) is very common during the solidification of steel.

Some thermodynamic and kinetic models for inclusion precipitation[12–14] have been proposed. However, only homogeneous nucleation has been considered in most of the models. Yang et al.[8] simulated the precipitation and growth of $MgAl_2O_4$-TiN complex inclusion during the solidification of bearing steel. Their model is mainly based on the thermodynamics of precipitation and does not include the kinetics of nucleation and growth. Descotes et al.[15] established a kinetic model for heterogeneous nucleation and growth of TiN on $MgAl_2O_4$ inclusions. The equation of crystal growth in their model is empirical, leading to the weak predictability of the model. In addition, some inaccuracy in the model can be attributed to the use of the equilibrium segregation model.

The present authors proposed a model for inclusion precipitation during steel solidification by combining Kampmann-Wagner numerical model (KWN) and the particle size grouping method.[16] The model has been applied in estimating the precipitation behavior of MnS and TiN and achieved very good performance in predicting the size distribution of precipitated inclusion. However, only homogeneous nucleation was accounted for in that model. In this work, we extend the model for describing the precipitation of TiN and TiN + oxide inclusions by considering both homogeneous and heterogeneous nucleation. TiN and TiN + oxide inclusions are precipitated from homogeneous and heterogenous nucleation, respectively, and the homogeneous and heterogeneous nucleation are considered to be competitive procedures in the model. The size distributions of both pure TiN from homogeneous nucleation and TiN + oxide from heterogeneous nucleation can be calculated from the model. The model was validated by the experimental data by Ohta et al.[17] The influence of various factors, e.g. nitrogen and titanium concentration, the interfacial tension between TiN and steel, cooling rate and number density of primary inclusions were investigated in the model calculations.

II. MODEL DESCRIPTION

The present model consists of a series of sub-models accounting for micro-segregation, heterogeneous nucleation and growth, homogeneous nucleation and growth and inclusion behavior at the solid-liquid interface. The supersaturation calculated by the micro-segregation sub-model is transferred to the sub-model of heterogeneous and homogeneous nucleation and growth. The heterogeneous and homogeneous nucleation and growth calculation are mainly based on the KWN model. To apply the KWN model in heterogeneous precipitation, the so-called "free-growth" model was employed for describing heterogeneous nucleation. The main assumptions related to the KWN model and micro-segregation calculation have been listed in our previous publication[16] and briefly listed as follows:

(1) The equilibrium partition coefficients of elements between solid and liquid steel are assumed to be constant during solidification.
(2) Spherical morphology of inclusion particles is assumed.
(3) The interfacial tension between inclusions and steel does not vary with the size of inclusions.
(4) Diffusion from bulk steel to interface is assumed to be controlling step for growth, coarsening of inclusions.

New assumptions associated with heterogeneous precipitation are as follows:

(1) The heterogeneous nucleation on primary oxide inclusions proceeds in a manner of instantaneous/athermal nucleation.[18]
(2) The homogeneous and heterogeneous nucleation mechanisms are considered to be competitive processes, and both are restricted by the concentration of solutes.
(3) Only growth is accounted for and the coarsening is neglected for heterogeneously precipitated inclusions. Since the heterogeneous precipitation only occurs on the particles larger than a critical size which is in the same value as the critical size for particle growth. It is reasonable to assume that the heterogeneous precipitated particles will merely grow.

The calculation procedure can be described by the flow chart of the present model calculation shown in Figure 1. The input data for the model calculation include steel composition, cooling rate and initial size distribution of oxide. The initial size distribution of oxide can be obtained by the experimental data or by the simulation for inclusion formation during steel refining. Firstly, the mass balance calculation is performed to calculate the liquid steel composition based on the total steel composition and inclusion size distribution. Secondly, the microsegregation calculation will be done to calculate the segregated solute concentrations in interdendritic liquid. Thirdly, the thermodynamic calculation will be preformed to determine if the inclusions can be precipitated due to the supersaturation. Finally, the

nucleation, growth and coarsening of inclusions will be calculated based on various nucleation mechanisms and KWN model.

The model calculations were executed in C++ programming. The calculation is very fast and the typical calculation duration is less than 600 seconds for a cooling rate as low as 0.8 K/s in an Intel core i5 laptop.

The sub-models will be introduced in the following sections. Since some of the sub-models are similar to that in our previous model, the description is brief to avoid repetition with a previous publication.[16]

A. *Microsegregation Calculation*

Ohnaka's equation[19] was employed to calculate the microsegregation of solute in residual liquid during the solidification of steel:

$$C_L = C_0(1 - \Gamma f_s)^{\frac{k-1}{\Gamma}} \text{ with } \Gamma = 1 - \frac{\alpha k}{1 + \alpha} \text{ and } \alpha = \frac{4Dt_f}{(\lambda_2)^2},$$

[1]

where f_s is the solidification fraction and can be calculated by the equation[13]: $f_s = \frac{(T_L - T)(1536 - T_S)}{(1536 - T)(T_L - T_S)}$ where T_L and T_S is the liquidus and solidus temperature for steel, respectively; C_L is the solute concentration in the residual liquid; C_0 is the initial concentration of solute. D is the diffusion coefficient of solute in solid; λ_2 is secondary dendrite arm spacing (SDAS); k is the equilibrium partition coefficient of the element between solid and liquid steel during solidification; t_f is local solidification time and can be expressed as: $t_f = \frac{T_L - T_S}{CR}$, and CR is the cooling rate (in K/s). The data of parameters of D and k can be found in Table I.

The liquidus temperature (T_L) and solidus temperature (T_S)—both in Celsius—of investigated steel can be calculated by the correlations proposed by Diederichs and Bleck[20]:

$$T_L = 1536 - 83[pct\ C] - 31.5[pct\ S] - 32[pct\ P] \\ - 5[pct\ Mn + pct\ Cu] - 7.8[pct\ Si] - 3.6[pct\ Al] \\ - 1.5[pct\ Cr] - 2[pct\ Mo] - 4[pct\ Ni] - 18[pct\ Ti] \\ - 2[pct\ V],$$

[2]

$$T_S = 1536 - 344[pct\ C] - 183.5[pct\ S] - 124.5[pct\ P] \\ - 6.8[pct\ Mn] - 12.3[pct\ Si] - 4.1[pct\ Al] \\ - 1.4[pct\ Cr] - 4.3[pct\ Ni].$$

[3]

Equations by Won and Thomas[21] are employed to calculate the SDAS of steel:

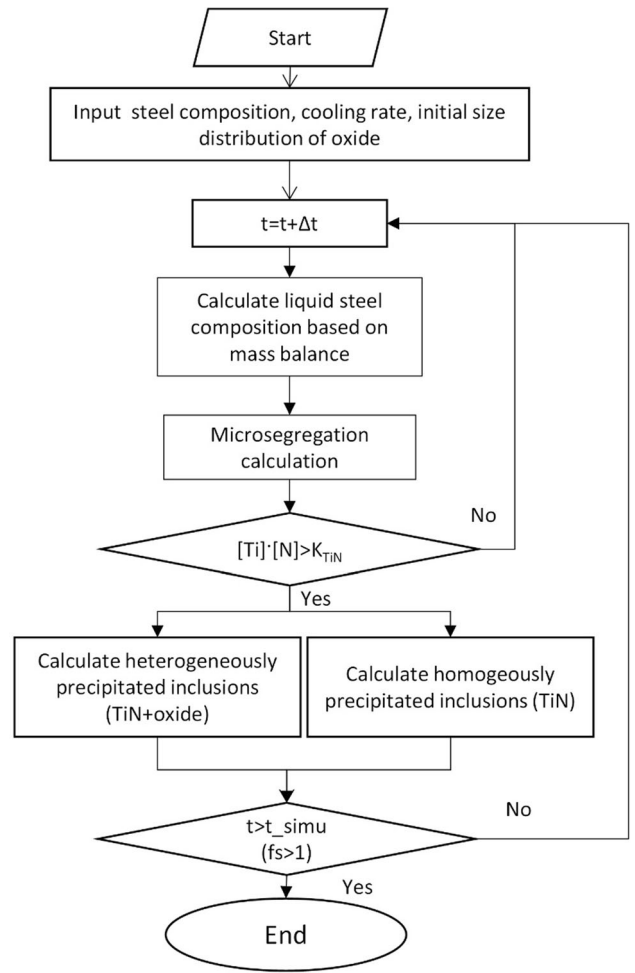$$\lambda_2 = (169.1 - 720.9[pct\ C])CR^{-0.4935}(0 < [pct\ C] < 0.15)$$

[4]

Fig. 1—Flow chart of the present model calculation (*t*: time; *t_simu*: total simulation time; Δt: time step; fs: solidification fraction).

$$\lambda_2 = 143.9[pct\ C]^{(0.5501 - 1.996[pct\ C])}CR^{-0.3616}([pct\ C] < 0.15)$$

[5]

where λ_2 represents secondary dendrite arm spacing (μm), and [pct C] is the mass percentage of carbon in steel.

B. *Heterogeneous and Homogeneous Nucleation*

The reaction for precipitation of TiN can be represented by: [Ti] + [N] = (TiN). The solubility product K_{TiN} is given by[22]:

$$log_{10}K_{TiN} = log_{10}([pct\ Ti][pct\ N]) = -\frac{14400}{T} + 4.94 \quad [6]$$

where T is the temperature in Kelvin. [pct Ti] and [N pct] are mass percentages of Ti and N in steel, respectively. The nucleation of TiN inclusions can be well described by the classic nucleation theory. The nucleation of inclusion during solidification can proceed in a homogeneous or heterogeneous manner. The steady-state nucleation rate for homogeneous

nucleation can be expressed as[23]:

$$I = I_A exp\left(-\frac{\Delta G^*_{hom}}{k_b T}\right),$$ [7]

where I_A is a pre-exponential factor, k_b is the Boltzmann constant (m^2 kg/s^2 K), and ΔG^*_{hom} is the free energy barrier (kJ/mol) for homogeneous nucleation:

$$\Delta G^*_{hom} = \frac{16\pi\sigma^3}{3\Delta G_V^2},$$ [8]

where σ is the interfacial tension (N/m) between inclusion and residual steel liquid; ΔG_V is Gibbs free energy change per molar volume for inclusion formation (kJ/m^3).

It has been introduced that some complex inclusions formed by the precipitation of secondary inclusions on some primary inclusions were frequently observed in many steel samples after solidification. For the sake of modelling the precipitation of secondary inclusions on existing primary oxides, it is assumed that a nucleus of secondary inclusion could form on the surface of the primary inclusions in liquid steel. The initial growth could be laterally but further growth would lead to the cover of the face of primary inclusions by secondary inclusion. This is termed "free growth" by Greer et al.[24] The critical condition for "free growth" is that the radius of the primary inclusions r should be equal to or larger than the critical radius for nucleation r_c: $r \geq r_c$, which is due to the geometric limitation. The critical radius for nucleation could be calculated by the following equation:

$$r_c = -\frac{2\sigma}{\Delta G_V}.$$ [9]

For the primary inclusions with a radius larger than the critical radius for nucleation, the secondary inclusions would nucleate on their surface. The nucleation energy barrier could be considered to be zero, and the nucleation rate could be infinitely large. Dantzig and Rappaz[18] also named this kind of heterogeneous nucleation "instantaneous nucleation". Since this kind of nucleation is not thermally activated, it is also termed "athermal nucleation". The precipitation kinetics of heterogeneous secondary inclusions should be determined by the consequent growth.

C. Kampmann-Wagner Numerical Model

According to the KWN model,[25,26] the nucleation, growth and coarsening of precipitates proceed concurrently. The treatment of heterogeneous and homogeneous nucleation of inclusion has been described in Section II–B. It should be mentioned that in the original KWN model, nucleation is treated only in homogeneous way. The present work has extended the KWN model to also depict heterogeneous nucleation.

Assuming that the crystal growth is controlled by diffusion in the boundary layer, the equation for the growth of crystals is as follows[27]:

$$v = \frac{dr}{dt} = \frac{\overline{C} - C_i}{C_P - C_i}\frac{D}{r},$$ [10]

where $\overline{C}$ is the concentration in residual liquid steel, C_p is the concentration in inclusion, C_i is the concentration at the interface, D is the diffusion coefficient (m^2/s) of the element in liquid steel, and r is the radius of the inclusion. The concentration C_i at the inclusion-steel interface is given by the Gibbs-Thomson equation:

$$C_i = C_e exp\left(\frac{2\sigma V_m}{rRT}\right)$$ [11]

where σ is the interfacial tension between inclusion and residual steel liquid, C_e is the equilibrium concentration.

The equation for the growth of crystals is satisfied for both homogeneous and heterogeneous nucleation. In the present heterogenous nucleation model, the secondary inclusion nucleates on primary inclusions larger than critical size and grows on the periphery of the core. The coarsening of particles for heterogeneous nucleation is neglected to keep the total number density of inclusions constant.

A finite volume method (FVM) suggested by Myhr et al.[28] is adopted for modelling the particle size distribution of inclusions using the KWN model. The size spectrum was discretized into a series of size groups. The size of particles in each group is increasing by R_r times compared with the size of particles in the previous group. $R_r = 2^{1/3}$ is adopted in this work. The growth and coarsening of crystals are treated by FVM method according to Patankar et al.[29] The detailed descriptions of the procedure and equations can be found in our previous publication.[16]

The agglomeration of inclusions due to Brownian collision in inter-dendritic liquid was considered in our previous model. The preliminary calculation indicates that the agglomeration of inclusions only has a negligible effect on the calculation results in the present work, and therefore the agglomeration of inclusion is neglected for the sake of simplification.

According to mass conservation law, the solute concentration in the inter-dendritic liquid can be calculated considering the precipitation of inclusions:

$$\overline{C} = \frac{C_0 - C_p\frac{\rho_{st}}{\rho_P}V_p}{1 - \frac{\rho_{st}}{\rho_P}V_p}$$ [12]

where V_p is the volume fraction of inclusions. V_p includes the contributions of volume fractions of homogeneous inclusions and heterogeneous nucleation: $V_p = V_{p,hm} + V_{p,ht}$ for homogeneously precipitated inclusions:

$$V_{p,hm} = \sum_{i=1}^{\infty}\frac{4}{3}\pi r_i^3 N_i$$ [13]

for heterogeneously precipitated inclusions:

Table I. The Data for Diffusion Coefficients of Solutes in δ-Fe and γ -Fe Phases and the Equilibrium Partition Coefficients Between Solid and Liquid During Solidification

	δ Phase		γ Phase	
Element	k	$D \times 10^4$ (m²/s)	k	$D \times 10^4$ (m²/s)
Ti	0.38	$3.15\exp(-247{,}693/RT)$	0.33	$0.15\exp(-250{,}956/RT)$
N	0.25	$0.008\exp(-79{,}078/RT)$	0.48	$0.91\exp(-168{,}490/RT)$

$$V_{\text{p,ht}} = \sum_{i=1}^{\infty} \frac{4}{3}\pi r_i^3 N_i - \sum_{i=1}^{\infty} \frac{4}{3}\pi r_{0i}^3 N_{0i} \quad [14]$$

where C_p represents the solute concentration in inclusions; C_0 is the initial solute concentration in inter-dendritic liquid steel, ρ_{st} and ρ_P represent the density (kg/m³) of liquid steel and inclusion, respectively, $r_{0,i}$ is the radius of primary oxide particles. N_{0i} is the number density of primary oxide particles with a radius of $r_{0,i}$

Depending on the cooling rates and relevant physical properties, the inclusions at the solid-liquid interface can be engulfed into the solid or pushed into the liquid.[30] A critical interface advancing velocity above which inclusions are engulfed in the solid steel can be defined according to previous studies. However, the critical velocity cannot be easily obtained due to the lack of accurate physical and thermodynamic properties of steel and inclusions. Instead, it is presumed in this work that the inclusions are engulfed in the solidified steel at a high cooling rate (higher than 10 K/s) and pushed into liquid at a low cooling rate (lower than 10 K/s). The pushed inclusions will undergo the nucleation, growth and agglomeration processes, while the engulfed inclusions in solid are assumed to be free of nucleation and growth.[16]

III. RESULTS AND DISCUSSION

A. *Validation of the Model*

Ohta *et al.*[17] studied the precipitation of TiN in Fe-1.5 pct Mn-0.05 pct C-0.1 pct Ti steel with and without Mg deoxidation. The inclusions were characterized by scanning electron microscopy (SEM). Their results can be employed to validate the present model for TiN precipitation.

The parameters used for calculating the size distribution of TiN in this work are as same as those in our previous publication.[16] It was assumed that all inclusions will be pushed into the inter-dendritic liquid steel at the cooling rates of 50 K/min.

As will be shown in Section III–F, the size distribution of primary oxides will critically influence the precipitation of secondary oxides. However, the data of the size distribution of MgO was not reported by Ohta *et al.*[17] Therefore, the size distribution of MgO after deoxidation was calculated by a model for nucleation, growth, coarsening and agglomeration of inclusions which was

proposed by the present authors.[31] The calculated size distribution of MgO at 600 seconds after deoxidation is shown in Figure 2. The model was originally proposed to describe the size distribution of alumina inclusions, but it is easy to extend the model for the formation of MgO inclusions. The model parameters for MgO deoxidation are shown in Table II. It should be mentioned that the agglomeration due to turbulent collisions is omitted in the model calculation since there was no stirring in the experiments by Ohta *et al*. The depth for inclusion floatation is assumed to be 0.03 m.

The size distributions of TiN + MgO inclusions in steels with different nitrogen concentrations after cooling are calculated by the present model and shown in Figure 2. The calculated mean sizes of inclusions are shown in Table III. The measured mean sizes are also shown in Table III for comparison. It can be seen that the calculated mean sizes of inclusions are in good agreement with the measured ones, indicating that the present model can reproduce the mean size of inclusions well. The mean absolute error (MAE) for the mean diameters is 0.15 μm.

B. *Effect of Nitrogen and Titanium Concentration*

The variation of titanium and nitrogen concentration in steel will change the supersaturation in residual liquid and affect the final size distribution of TiN and TiN + MgO inclusions. The effects of both nitrogen and titanium concentration on the final size distribution of TiN and TiN + MgO are studied by model calculation.

The calculated size distributions of TiN + MgO in steel with 70, 120, 130 and 160 ppm [N] are shown in Figure 2, while the size distribution of pure TiN in steel with 120, 130 and 160 ppm [N] is shown in Figure 3. It should be mentioned that there is no precipitation of pure TiN in steel with 70 ppm [N]. As seen in Figure 3, as nitrogen concentration rises from 120 to 130 ppm, the maximum number density of TiN increases and the radius at the maximum peak remains nearly unchanged. Further increase of nitrogen concentration increases the maximum number density of pure TiN and decreases the radius at the maximum peak. The increased number density at higher nitrogen concentration should be due to the enhanced nucleation generated by larger supersaturation. Lee and Park[35] characterized TiN and TiN + oxide inclusions in ferritic stainless steel and found that the number density of TiN increases accordingly as the nitrogen concentration increases. Heikkinen *et al.*[34] investigated the type of inclusions in the

austenitic stainless steel grade 316Ti. The formation of TiN inclusions was found to be pronounced in cases with high Ti and N contents. Our calculation is in accordance with their results.

It can be seen in Figure 2 that the size distribution of TiN + MgO firstly moves towards the larger size as nitrogen content increases from 70 to 130 ppm. Some parts of small inclusions (with a radius less than 50 nm) for 70 ppm [N] fit well with the size distribution of MgO, reflecting that some MgO inclusions are not covered by TiN. The results suggest that MgO inclusions smaller than 50 nm are not activated for nucleation due to their small size. This phenomenon is not found in the size distribution of steels with 120 ppm and 130ppm [N]. Since the Gibbs energy change for inclusion nucleation increases with nitrogen concentration, the critical size of MgO for heterogeneous nucleation decreases, as shown in Eq. [9]. Therefore, no inactivated MgO is found in the size distribution of inclusions in steel with 120 and 130 ppm.

Further increase of nitrogen to 160 ppm leads to the dramatic increase of the number density of small TiN + MgO inclusion particles, indicating that the heterogeneous nucleation is largely suppressed. This corresponds to the large increase in the number density of TiN shown in Figure 3 and can be attributed to the competition between heterogeneous and homogeneous nucleation. The increase of nitrogen concentration can increase the supersaturation degree and is favorable to the homogeneous nucleation. The well-developed homogeneous nucleation, in turn, suppressed the heterogeneous nucleation, leading to the size decrease of TiN + MgO inclusions.

The size distributions of pure TiN and TiN + MgO inclusions in steel with 0.05, 0.07, 0.1, 0.13 and 0.15 pct Ti are calculated by the present model and shown in Figure 4. The nitrogen concentration is kept constant at 110 ppm. No homogeneous precipitation of TiN is found in steels with 0.05 and 0.07 pct Ti. It can be seen in the figure that the effect of titanium concentration on

size distribution is very similar to that of nitrogen concentration. The homogeneous nucleation of TiN inclusion is enhanced by the increase of titanium concentration due to the enhanced supersaturation. The maximum number density of TiN inclusions is the highest for the steel with maximum titanium concentration. Both size distributions of TiN + MgO inclusions in steels with 0.05 and 0.07 pct Ti have some parts overlapping with that of MgO, indicating some MgO inclusions are not activated. As titanium concentration increases to 0.1 pct, no inactivated MgO is found in the size distribution. The explanation can be similar to that for nitrogen concentration variation. Both nitrogen and titanium concentrations affect the supersaturation of TiN precipitation. The increase of titanium concentration will also decrease the critical size for heterogeneous nucleation, and therefore no inactivated MgO is found in steel with a larger amount of Ti. The heterogeneous precipitation of TiN + MgO is suppressed due to the developed homogeneous precipitation of TiN as the titanium concentration increases from 0.1 to 0.13 pct. Further increase of titanium to 0.15 pct leads to the significantly suppressed heterogeneous precipitation.

It has been shown that the effect of nitrogen and titanium concentration on inclusion size distribution can be mainly attributed to the change of supersaturation($[Ti] \cdot [N]/K_{TiN}$). It will be interesting to investigate the effect of the ratio of titanium to nitrogen concentration ($[Ti]/[N]$) on the size distribution of inclusions under the constant $[Ti] \cdot [N]$ values. Figure 5 illustrates the size distribution of pure TiN and TiN + MgO inclusions in steel with $[Ti]/[N]$ = 5, 10 and 20 calculated by the present model. The increase of the $[Ti]/[N]$ ratio suppresses the heterogeneous nucleation of TiN + MgO inclusions and promotes the homogeneous nucleation of TiN inclusions. This could be due to the fact that the diffusion of nitrogen is considered to be the controlling step for the growth of TiN + MgO inclusions. As the $[Ti]/[N]$ ratio rises, the nitrogen concentration decreases and the diffusion of nitrogen was weakened. Accordingly, the heterogeneous nucleation of TiN + MgO is suppressed, and as the competitor of heterogeneneous nucleation, homogeneous nucleation of TiN is promoted (Figure 5).

C. Effect of Interfacial Tension Between TiN and Steel

It was revealed in our previous studies that the interfacial tension between inclusion and steel can have an impact on the homogenous nucleation, growth and coarsening of inclusions.[16] In this work, the effects of interfacial tension between TiN and steel on both the heterogeneous and homogenous nucleation are investigated by the model calculations. The size distributions of TiN + MgO and pure TiN inclusions with interfacial tension values of 0.20, 0.25, 0.28 and 0.30 N/m were calculated by the present model and shown in Figure 6. The steel composition of MT-1 in Table III was employed for this calculation and thereafter. As can be seen in Figure 6(a), the interfacial tension between TiN and steel has an impact on the size distribution of pure TiN inclusions. As the interfacial tension increases from
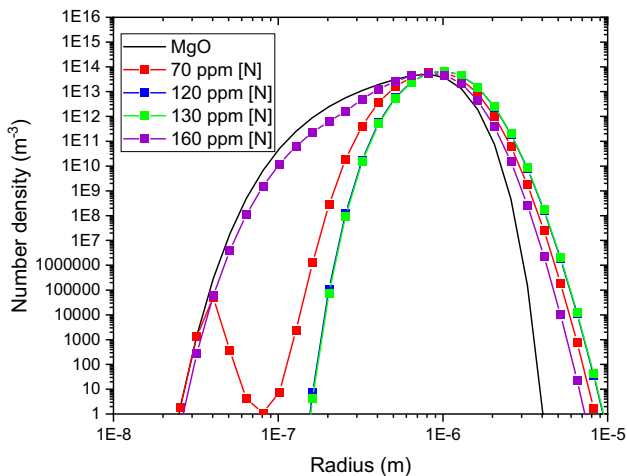

Fig. 2—The calculated size distributions of TiN + MgO inclusions in steel with various nitrogen concentrations after solidification with a cooling rate of 0.83 K/s.

Table II. Physical and Thermodynamic Properties for Simulating the Size Distribution of MgO Inclusions[31,32]

Physical Properties	Value	Unit
Density of Liquid Steel	7000	kg/m^3
Density of MgO Inclusions	3823	kg/m^3
Molar Mass of MgO	0.0403	kg/mol
Dynamic Viscosity of Liquid Steel	0.0067	Pa.s
Diffusion Coefficient of Oxygen in Steel Melts at 1873 K	2.7×10^{-9}	m^2/s
Interfacial Tension Between MgO and Steel Melt	0.5	N/m
Equilibrium Constant for Mg + O = MgO at 1873 K	$10^{7.74}$	
Temperature	1873	K

Table III. Comparison Between Calculated and Measured[17] Mean Diameters of Inclusions in Fe-Mn-Ti-N Steels

	Steel Composition					Mean Diameter	
No.	[C] pct	[N] ppm	[Mn] pct	[Si] pct	[Ti] pct	Measured (μm)	Calculated (μm)
MT-1	0.05	119	1.5	0	0.12	1.83	2.04
MT-2	0.05	112	1.53	1.08	0.12	1.91	2.00
MT-3	0.05	70	1.55	0	0.12	1.95	1.836
MT-4	0.05	69	1.51	1.05	0.12	1.80	1.832
MT-5	0.15	122	1.53	0	0.12	2.03	1.94
MT-6	0.15	130	1.50	1.05	0.12	2.09	1.73
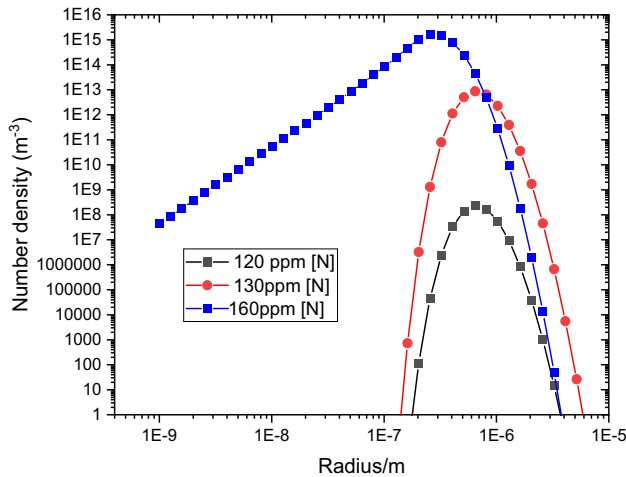
Fig. 3—The calculated size distribution of pure TiN inclusions precipitated in the steel with various [N] concentrations.

0.20 to 0.30 N/m, the maximum number density of inclusions dramatically decreases from 1.86×10^{15} to 3606.6 m^{-3}. At first, the radius at maximum peak rapidly increases and then remains nearly the same as the interfacial tension increases. This is in line with our previous model calculations on homogeneous nucleation of TiN.[16] The continuous decrease of maximum number density in the size distribution of pure TiN with increasing interfacial tension should be due to the suppressed nucleation by enhanced energy barrier for homogeneous nucleation. According to Eq. [8], the Gibbs free energy barrier for homogeneous nucleation is

proportional to the cubed interfacial tension between inclusion and steel radius at the maximum peak increase of TiN inclusions with increasing interfacial tension can be attributed to the enhanced coarsening and can be further explained by Lifshitz-Sloyzov-Wagner (LSW) theory.[35,36] According to LSW theory, the growth of the mean diameter of particles due to coarsening can be expressed by the following equation by assuming diffusion is the controlling step:

$$\overline{d}^3 - \overline{d}_0^3 = kt = \frac{64 D \sigma V_m c_0}{9RT} t, \quad [15]$$

where k is coarsening rate; $\overline{d}$ and $\overline{d}_0$ are the mean size at time t and initial mean size, respectively; V_S is the molar volume of crystal; c_0 is the equilibrium mass concentration of mobile species in liquid. The coarsening rate k is directly proportional to the interfacial tension between inclusion and steel. As the interfacial intension increases, the coarsening is enhanced and the mean size of inclusion increases.

It can be seen in Figure 6(b) that the size distribution of TiN + MgO inclusions only slightly changes as the interfacial intension decreases from 0.30 to 0.28 N/m. However, the further decrease of interfacial intension to 0.25 N/m will lead to a critical increase in the number density of small particles and a decrease in the number density of large particles. This indicates that the heterogeneous nucleation is suppressed by reducing interfacial tension. In the present model, the heterogeneous nucleation on the primary inclusion is competing with the homogeneous nucleation. The reduced interfacial tension will be favorable to the homogeneous
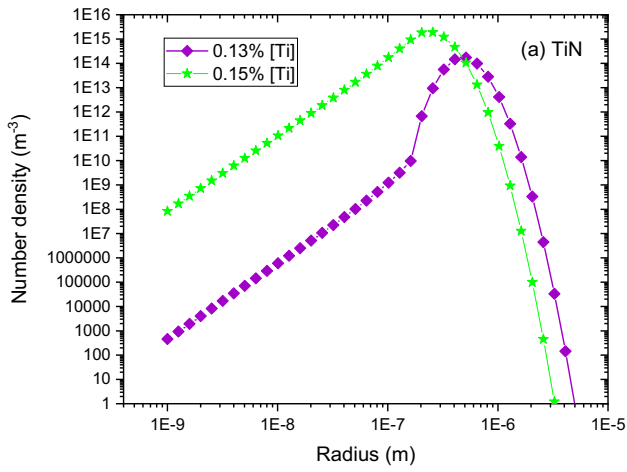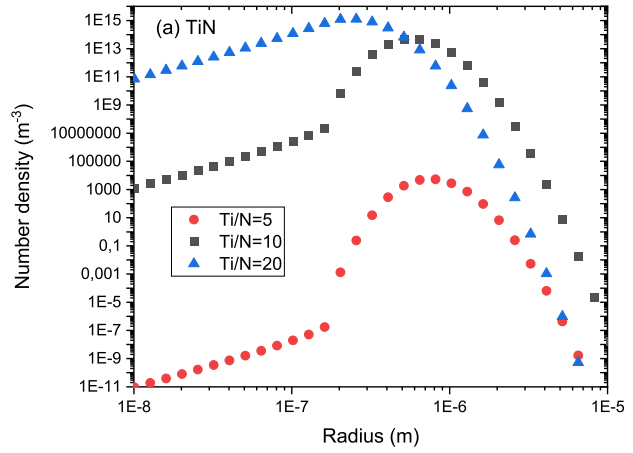
(a)
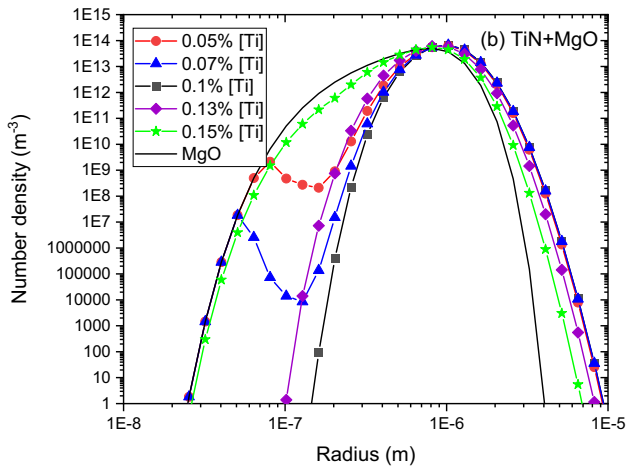
(b)

Fig. 4—The calculated size distribution of (*a*) pure TiN and (*b*) TiN + MgO inclusions precipitated in the steel with [N] = 110 ppm and various [Ti] concentrations.

nucleation, and then the well-developed homogeneous nucleation will further suppress the heterogeneous nucleation.

D. Effect of the Cooling Rate

It has been found that the precipitation of TiN inclusion is critically influenced by the applied cooling rate. An inverse linear relationship between the size of particle and the logarithm of cooling rate was established for precipitation of TiN by the previous studies.[37–40] The present authors investigated the effect of cooling rate on homogeneous nucleation and growth and found the size of inclusions decreases with increasing cooling rate.[16] However, these studies are mainly focused on the precipitation of pure TiN inclusions. There are very few investigations on the effect of cooling rate on the precipitation of complex TiN + oxide inclusions. The effect of cooling rate on the precipitation of both complex TiN + MgO and pure TiN was studied by the present model calculation.

(a)
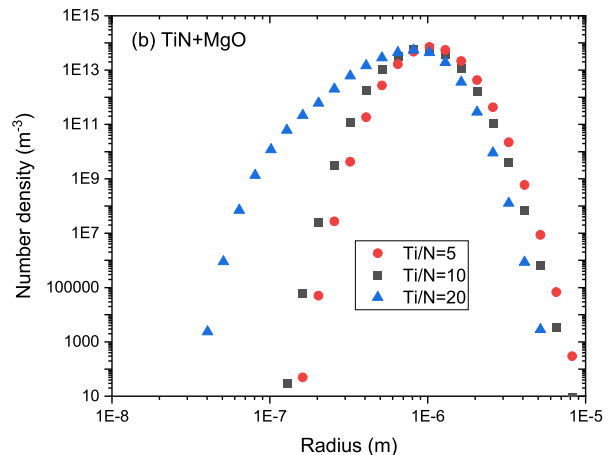
(b)

Fig. 5—The calculated size distribution of (*a*) pure TiN and (*b*) TiN + MgO inclusions precipitated in the steel with [Ti][N] = 0.00144 and various [Ti]/[N] ratios.

The size distributions of complex TiN + MgO and pure TiN in steel cooled at rates of 16.6, 8.3, and 0.83 K/ s are calculated by the present model and shown in Figure 7. It should be considered that the inclusions can have different behaviors at the solidifying interface at the different cooling rates. Therefore, the size distribution of inclusions are calculated both for pushing and engulfment cases. It can be seen from Figure 7(a) that the maximum number density of pure TiN increases as the cooling rate increases. This might be due to the fact that the microsegregation of Ti and N is enhanced by the increasing cooling rate. The increasing Ti and N in the inter-dendritic liquid will raise the supersaturation for TiN precipitation and thereby increase the number density of TiN in steel. Nevertheless, the effect of cooling rate on the TiN precipitation with both heterogeneous and homogeneous nucleation is much weaker than that on TiN precipitation with only homogeneous nucleation. Figure 7(c) also shows a similar trend of maximum number density as Figure 7(a). Besides, the increase in the number of small inclusions at a high cooling rate is even more obvious.
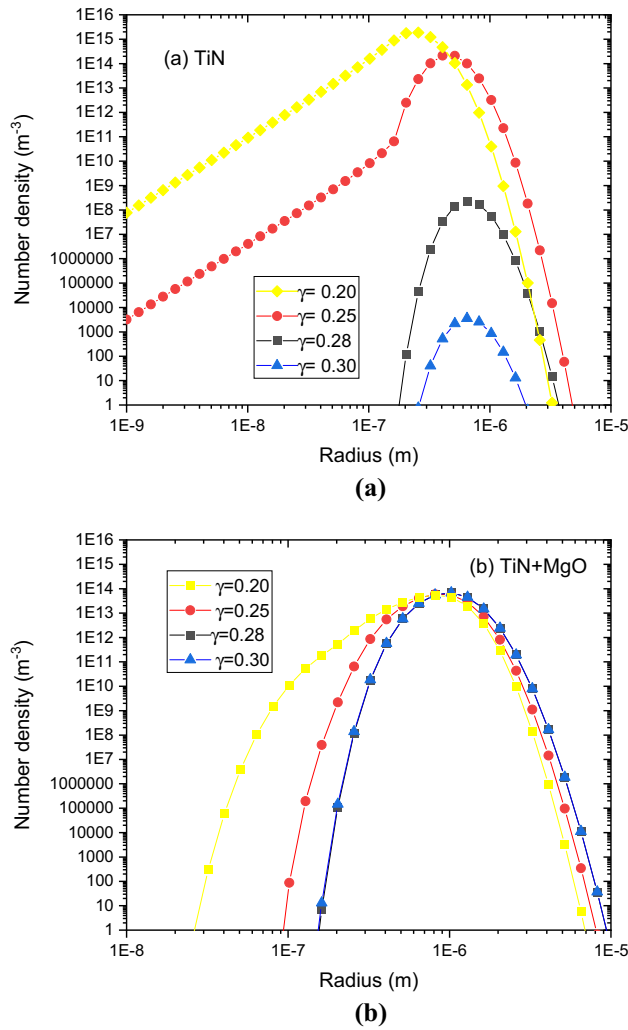
(a)

(b)

Fig. 6—The calculated size distribution of (*a*) TiN and (*b*) TiN + MgO inclusions after solidification of steel with various interfacial tension values between steel and inclusions.

As can be seen in Figure 7(b), the size distribution of TiN + MgO is barely affected by the cooling rate. Only a slight increase in the number of large inclusions can be found in the model calculation for a low cooling rate. It is found in Figure 7(d) that there are some increases in number density values of small inclusions at a higher cooling rate but generally the influence of cooling rate is still minor for the case of inclusion engulfments.

E. *Effect of Engulfment and Pushing*

Depending on the cooling rate applied, the inclusion at the liquid/solid interface could be engulfed into the solidified steel or pushed back into liquid, which could influence the size distribution of inclusion in the final solidified steel. There are already some mathematical models[41] to calculate the critical interface velocity under which the inclusion will be pushed back. However, due to the lack of reliable physical properties and especially interfacial properties, it is not easy to calculate the critical interface velocity for the specific steels and

inclusions. Accordingly, the size distributions of MgO + TiN inclusions in solidified steel at the cooling rate of 8.6 K/s are calculated both in the engulfment and pushing case to check if the behavior of inclusion at the solid-liquid interface will bring a large influence on the final size distributions of inclusions. The calculated size distributions of inclusions by assuming engulfment and pushing of inclusions are shown in Figures 8(a) and (b) respectively. Compared with the size distribution under the assumption of inclusion pushing, the size distribution produced by inclusion engulfment is much wider. This is due to the fact that many fine inclusions engulfed in the solidified steel have no opportunity to grow and coarsen. In the case of pushing, the inclusions are pushed to the residual liquid and subject to the coarsening process, which will lead to the decrease of total number density due to the diminishing of small inclusions. The coarsening and growth of TiN and TiN + MgO are much more developed in the pushing case than in the engulfment case.

F. *Effect of Size Distribution of Primary Inclusions*

It is well accepted that the size distribution of inclusions undergoing nucleation, growth and coarsening will follow a log-normal distribution.[31,42] Assuming a log-normal distribution, the number density of primary MgO inclusions can be calculated as follows:

$$n(r) = \frac{N_0}{\sigma r \sqrt{2\pi}} exp\left(-\frac{(ln(r) - ln(r_0))^2}{2\sigma^2}\right), \quad [16]$$

where r and r_0 are the radius and mean radius of inclusion particles, respectively; σ^2 is the variance, and the maximum density is given by $\frac{N_0}{\sigma r \sqrt{2\pi}}$.

The effect of the size of primary MgO inclusions on the size distribution of heterogeneous inclusions was investigated by assuming three size distributions of primary inclusions with mean radii of 0.3, 0.5 and 0.8 μm, assuming $\sigma = 0.2$. To keep the maximum density unchanged, the N_0 was set to be 6×10^4, 1×10^5 and 1.6×10^5, respectively. The size distributions of pure TiN and heterogeneous TiN + oxide inclusions are calculated by the present model and shown in Figure 9. For the sake of comparison, the initial size distributions of primary oxide inclusions are also shown in Figure 9(a). It can be seen that the size distribution of TiN + oxide only has a very weak dependence on the size of primary oxide inclusions. The size distributions of TiN + oxide nucleating on primary oxide inclusions with varying sizes are very close to each other. This might be due to the fact that the inclusions with smaller sizes have a larger growth rate as shown in Eq. [10], which leads to the very close final inclusion size distribution.

As shown in Figure 9(b), the size distribution of TiN inclusions coexisting with TiN + oxide also shows similar behavior. The size of primary oxide inclusions has almost no influence on the size distribution of precipitation TiN inclusions.
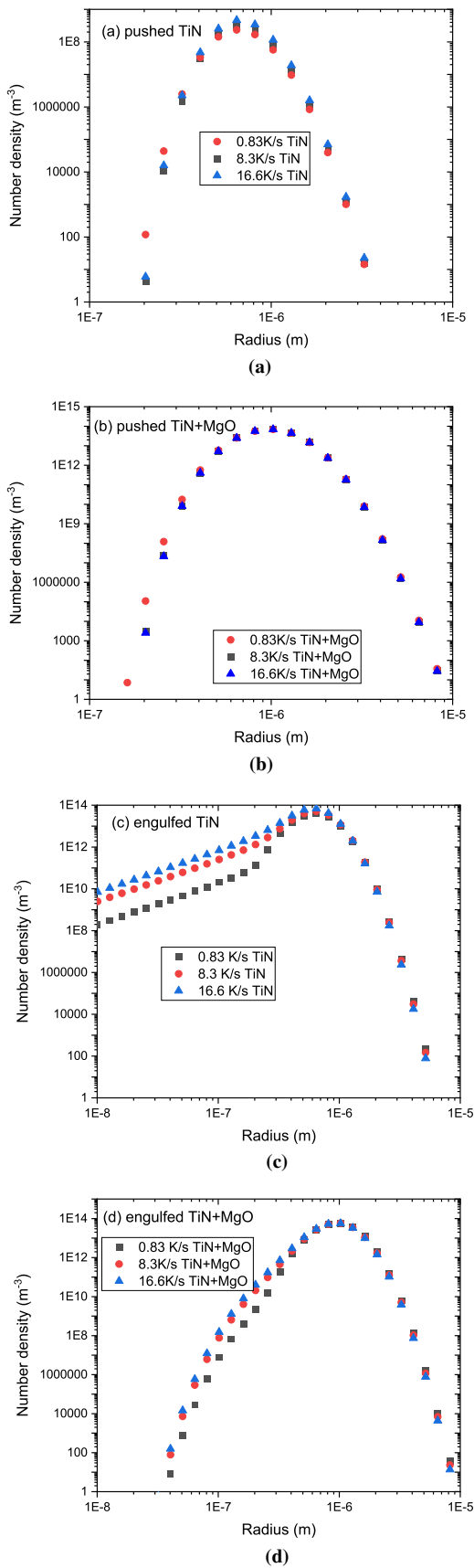
(a)

(b)

(c)

(d)

Fig. 7—The calculated size distribution of (*a*) pushed TiN and (*b*) pushed TiN + MgO (*c*) engulfed TiN and (*d*) engulfed TiN + MgO inclusions in steel cooled with various rates.
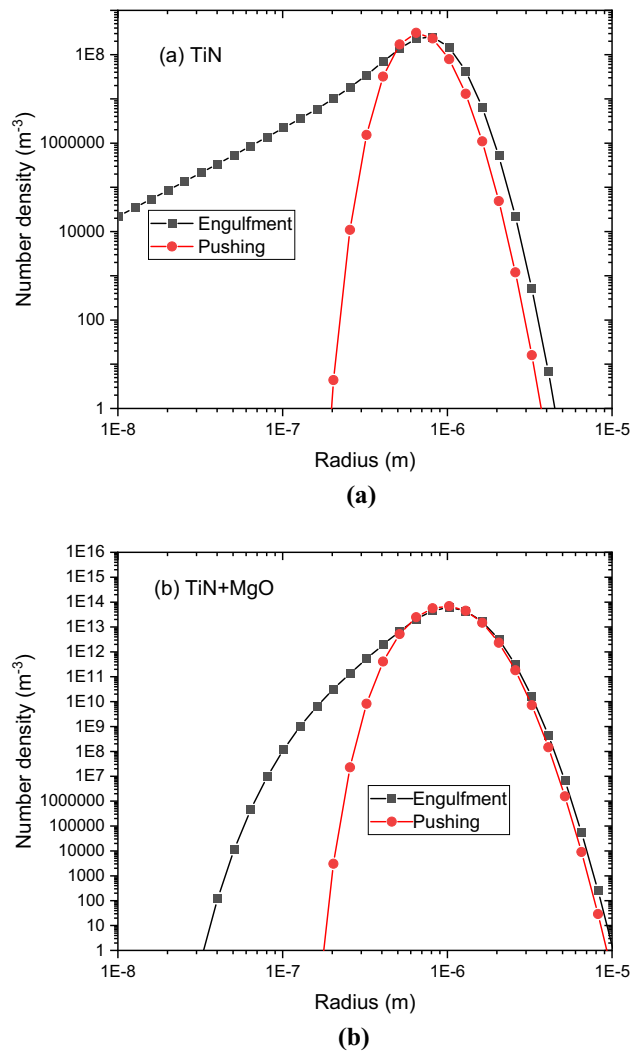

(a)

(b)

Fig. 8—The calculated size distributions of (*a*) TiN and (*b*) TiN + MgO by assuming engulfment and pushing of inclusions.

The effect of the maximum number density of MgO on the size distribution of TiN and TiN + MgO was further studied by assuming $N_0 = 1 \times 10^5$, 1×10^7, 1×10^{10}. The calculated size distributions of TiN and TiN + MgO inclusions are shown in Figure 10. No precipitation of pure TiN was found in cases with $N_0 = 1 \times 10^{10}$. It can be seen in the figure that the maximum number density of TiN + MgO increases with increasing the maximum number density of MgO. Meanwhile, the mean size of TiN + MgO is reduced by increasing the maximum number density of MgO. The effect of primary oxide number density on the final TiN + oxide was investigated by Descotes *et al*[15] using model calculation. They also observed similar results that inclusion size decreases as the number density of primary oxide increases. The increased number density of MgO as heterogeneous nucleation sites enhances the heterogeneous nucleation of TiN and leads to the faster depletion of supersaturated nitrogen and titanium. As a result, the growth of TiN on primary oxide is restricted

and the final size of TiN + MgO inclusions decreases. The increase in the number density of MgO also has an impact on the homogeneous nucleation. As N_0 increases from 1×10^5 to 1×10^7, both the maximum number density and radius at the maximum peak decrease. Further increase of N_0 will diminish the precipitation of pure TiN. These results indicate that the homogeneous nucleation can be significantly suppressed by adding a large number of particles as heterogeneous nucleation sites. Pervushin et al.[10] investigated the effect of the number of oxide particles on the final TiN and TiN + oxide inclusions. They found that the number of TiN + oxide increases and the number of TiN decreases as the number of oxide particles increases. The ratio of the number of TiN to TiN + oxide decreases with an increasing number of oxide particles. Their experimental results are in line with our calculation results.
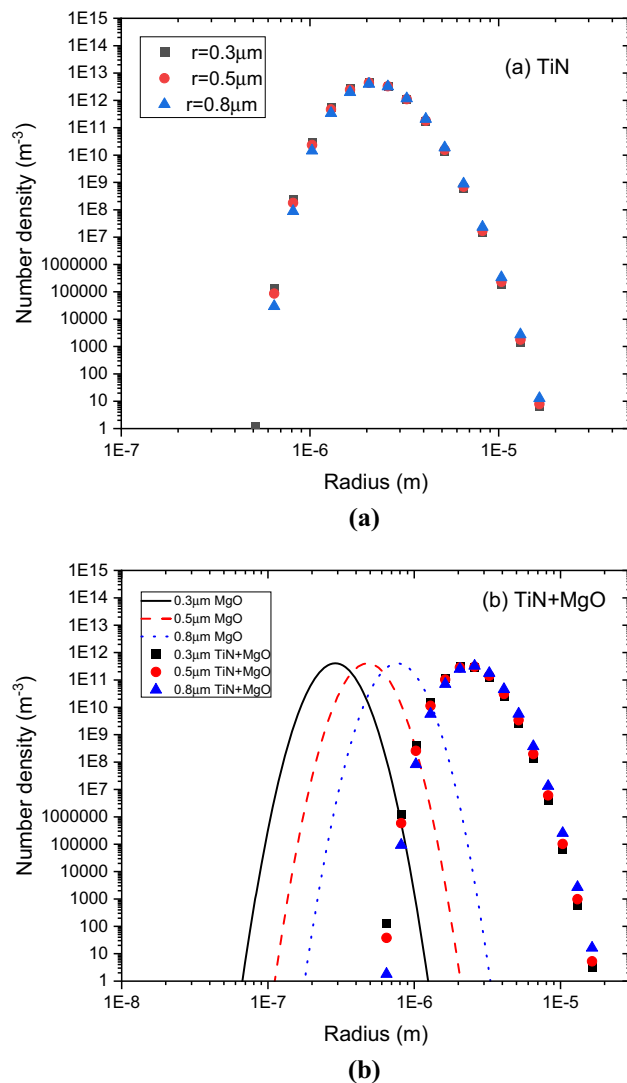
G. Discussion on Inclusion Control

The oxide metallurgy requires the fine size of inclusions to act as the nucleation sites to promote the formation of acicular ferrite. To alleviate the detrimental effect of inclusions on the properties of steel, the size and number of inclusions should be reduced. The calculation results by the present model can provide clues to optimize the process for controlling the size distribution of inclusions.

It has been found that the concentration of nitrogen and titanium, the interfacial tension between steel and inclusions, and the number density of primary MgO inclusions all impact the final size distribution of inclusions. In comparison, the cooling rate and the size of primary MgO inclusions have only minor effects. The concentration of nitrogen and titanium cannot be readily changed due to the steel grade requirements, while the interfacial tension between steel and inclusion

Fig. 9—The size distribution of inclusions in solidified steel with various sizes of MgO particles (a) TiN (b) TiN + MgO.
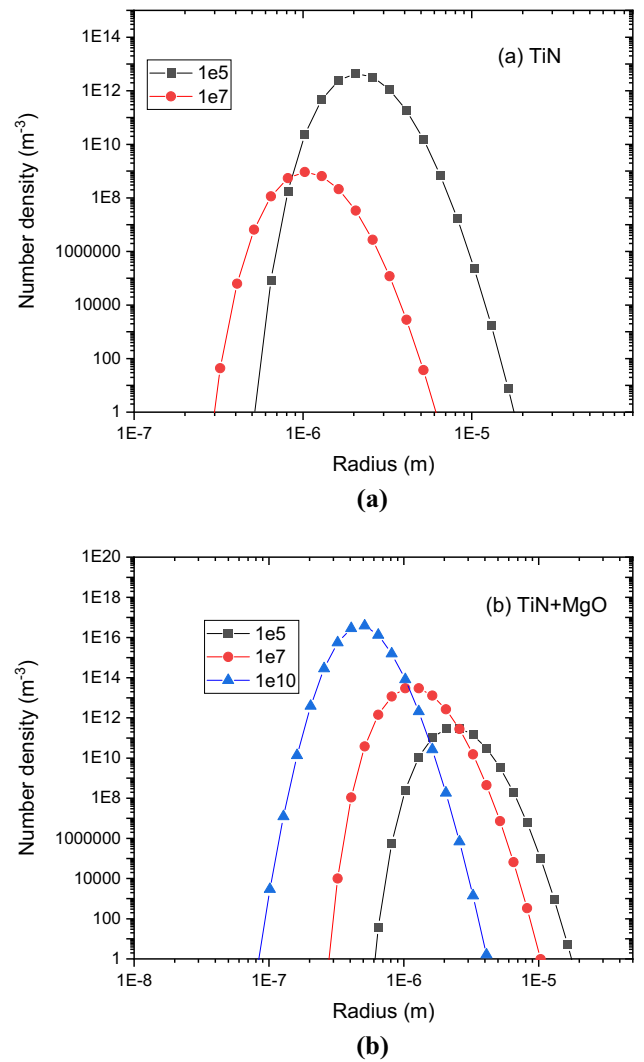

Fig. 10—The calculated number density of (a) TiN and (b) TiN + MgO inclusions with different maximum number density values of MgO particles.

and the number density of primary inclusions can be parameters for controlling the inclusions in steel after solidification.

The interfacial tension between TiN and steel can be varied with the concentration change of surface-active elements, *e.g.* O and S, in steel. It can be obtained from the present calculation in Section III–C that larger interfacial tension between TiN and steel would suppress the homogeneous nucleation and will be favorable to heterogeneous nucleation. In contrast, the smaller value of interfacial tension will promote homogeneous nucleation (see Figure 6). The interfacial tension between TiN and steel can be adjusted by changing steel composition to control the precipitation of TiN inclusions.

The increase in the number density of primary oxide can significantly suppress the homogeneous nucleation and reduce the size of TiN + oxide inclusions. Therefore, the large number of primary oxide will be favorable to the precipitation of small-size heterogeneous TiN + oxide inclusions, which could act as the nucleation sites for fine intragranular acicular ferrite.

The present model can be extended to describe the precipitation of other complex inclusions. The most important assumption for this model is that heterogeneous nucleation proceeds in the manner of instantaneous or athermal nucleation, which requires very good compatibility between secondary inclusions and the primary inclusion substrate. The ability of oxide substrate to act as a heterogeneous nucleation site for TiN can be reflected by the lattice misfit parameter δ[43] between oxide and TiN which is expressed by the following equation:

$$\delta = \frac{\left|l_{MxOy} - l_{TiN}\right|}{1/2(l_{MxOy} + l_{TiN})} \qquad [17]$$

where l_{MxOy} and l_{TiN} are distances between neighboring atoms for various lattice orientations in oxide and TiN, respectively. The δ between TiN and MgO can be as low as 0.0002, indicating that MgO can be a very effective heterogeneous nucleation site for TiN. Other oxides with low lattice misfit parameters, *e.g.* Ce_2O_3 and $MgAl_2O_4$ can be also excellent candidates for inducing heterogeneous nucleation.

The knowledge of the size distribution of primary oxide is essential to describing and modelling the final size distribution of inclusions in steel after solidification. The primary oxide inclusion mainly stems from deoxidation and undergoes nucleation, growth, coarsening and agglomeration. A model combining Kampmann-Wagner numerical model with the population balance equation solved by the particle size grouping method has been proposed by us to calculate the evolution of primary oxide inclusions.[31] This model has been applied to calculate the size distribution of MgO in this work. This also indicates that model for the evolution of inclusions through processes from deoxidation to solidification and even reheating will be imperative to describe and calculate accurately the size distribution of inclusions in final products.

IV. CONCLUSIONS

A model accounting for both heterogeneous and homogeneous nucleation was proposed for describing the precipitation kinetics of TiN and complex TiN + MgO inclusions. The model has been validated by the experimental data in the literature. The influence of various factors, such as titanium and nitrogen concentration, cooling rates, interfacial tension, and size distribution of primary oxides have been investigated by the model calculation. Based on the results of this study, the following conclusions were drawn:

(1) As the concentration of Ti and N increases, the maximum number density of pure TiN increases. At the low concentration of Ti and N, some of the MgO inclusions are not activated for heterogeneous nucleation. With an increase of Ti and N, all MgO inclusions are activated and heterogeneous nucleation is enhanced. However, further increase of Ti and N will suppress the heterogeneous precipitation due to the well-developed homogeneous nucleation.

(2) The interfacial tension between TiN and steel has an impact on the precipitation of TiN and TiN + MgO inclusions. As interfacial tension increases, the homogeneous precipitation of TiN is suppressed, while the heterogeneous precipitation of TiN + MgO is enhanced.

(3) The influence of the applied cooling rate of steel solidification on the final size distribution of precipitated TiN and TiN + MgO inclusions is negligible.

(4) The initial size of primary oxide particles has only a slight effect on the final size distribution of TiN and TiN + MgO inclusions. The number density of primary oxide particles has an impact on both heterogeneous and homogenous nucleation and growth of TiN and TiN + MgO inclusions. The increasing number density of primary oxide particles will suppress the homogeneous nucleation of TiN and decrease the size of heterogeneous TiN + MgO inclusions.

CONFLICT OF INTEREST

The authors declare no conflict of interest.

REFERENCES

1. Holappa and O. Wijk: Inclusion Engineering, in S. Seetharaman, A. McLean, R. Guthrie and S. Sridhar (eds), Treatise on Process Metallurgy, Volume 3: Industrial Processes, 2014. pp. 347–72.
2. T. Uesugi: *Trans. ISIJ*., 1986, vol. 26, pp. 614–20.
3. T.Y. Jin, Z.Y. Liu, and Y.F. Cheng: *Int. J. Hydrogen Energy*., 2010, vol. 35, pp. 8014–21.
4. T. Yamada, H. Terasaki, and Y.I. Komizo: *ISIJ Int*., 2009, vol. 49, pp. 1059–62.
5. P.R. Scheller and Q. Shu: *Steel Res. Int*., 2014, vol. 85, pp. 1310–16.
6. S.K. Choudhary and A. Ghosh: *ISIJ Int*., 2009, vol. 49, pp. 1819–27.
7. D. You, S.K. Michelic, P. Presoly, J. Liu, and C. Bernhard: *Metals*., 2017, vol. 7, p. 460.
8. L. Yang, G.G. Cheng, S.J. Li, M. Zhao, and G.P. Feng: *ISIJ Int*., 2015, vol. 55, pp. 1693–98.
9. Q. Tian, G. Wang, Y. Zhao, J. Li, and Q. Wang: *Metall. Mater. Trans. B*., 2018, vol. 49B, pp. 1149–64.
10. G.V. Pervushin and H. Suito: *ISIJ Int*., 2001, vol. 41, pp. 748–56.
11. M. Alba, M. Nabeel, and N. Dogan: *Steel Res. Int*., 2020, vol. 91, p. 1900477.
12. P. Rocabois, J. Lehmann, H. Gaye, and M. Wintz: *J. Cryst. Growth*., 1999, vol. 198, pp. 838–43.
13. Z. Ma and D. Janke: *ISIJ Int*., 1998, vol. 38, pp. 46–52.
14. D. You, S.K. Michelic, G. Wieser, and C. Bernhard: *J. Mater. Sci*., 2017, vol. 52, pp. 1797–1812.
15. V. Descotes, T. Quatravaux, J.P. Bellot, S. Witzke, and A. Jardy: *Metals*., 2020, vol. 10, p. 541.
16. Q. Shu, V.-V. Visuri, T. Alatarvas, and T. Fabritius: *Metall. Mater. Trans. B*., 2020, vol. 51, pp. 2905–16.
17. H. Ohta and H. Suito: *ISIJ Int*., 2007, vol. 47, pp. 197–206.
18. J.A. Dantzig and M. Rappaz: Solidification: -Revised & Expanded. EPFL Press; 2016 Nov 18.
19. I. Ohnaka: *Trans. ISIJ*., 1986, vol. 26, pp. 1045–51.
20. R. Diederichs and W. Bleck: *Steel Res. Int*., 2006, vol. 77, pp. 202–09.
21. Y.M. Won and B.G. Thomas: *Metall. Mater. Trans. A*., 2001, vol. 32A, pp. 1755–67.
22. H. Wada and R.D. Pehlke: *Metall. Trans. B*., 1985, vol. 16B, pp. 815–22.
23. D. Turnbull: *J. Chem. Phys*., 1952, vol. 20, pp. 411–24.
24. A.L. Greer, A.M. Bunn, A. Tronche, P.V. Evans, and D.J. Bristow: *Acta Mater*., 2000, vol. 48, pp. 2823–35.
25. J.S. Langer and K. Schwartz: *Phys. Rev. A*., 1980, vol. 21, p. 948.
26. R. Kampmann and R.Wagner: Decomposition of alloys: The early stages, Second Acta Scripta Metallurgica Conference, Pergamon Press, Sonnenberg, 1983, pp. 91–103.
27. H.B. Aaron, D. Fainstein, and G.R. Kotler: *J. Appl. Phys*., 1970, vol. 41, pp. 4404–10.
28. O.R. Myhr and Ø. Grong: *Acta Mater*., 2000, vol. 48, pp. 1605–15.
29. S.V. Patankar: *Numerical Heat Transfer and Fluid Flow*, Hemisphere, Washington, DC, 1980.
30. H. Shibata, H. Yin, S. Yoshinaga, T. Emi, and M. Suzuki: *ISIJ Int*., 1998, vol. 38, pp. 149–56.
31. Q. Shu, T. Alatarvas, V.-V. Visuri, and T. Fabritius: *Metall. Mater. Trans B*., 2021, vol. 52B, pp. 1818–29.
32. E.T. Turkdogan: *Physical Chemistry of High Temperature Technology*, Academic Press, Philadelphia, 1980.
33. M.H. Lee and J.H. Park: *Metall. Mater. Trans. B*., 2018, vol. 49B, pp. 877–93.
34. E.-P. Heikkinen, J. Savolainen, T. Ikäheimonen, V.-V. Visuri, and T. Fabritius: Proceedings of the 8th International Conference on Clean Steel, Hungarian Mining and Metallurgical Society, Budapest, Hungary, pp. 316–29, 2012.
35. I.M. Lifshitz and V.V. Slyozov: *J. Phys. Chem. Solids*., 1961, vol. 19, pp. 35–50.
36. C. Wagner: *Ber. Bunsenges. Phys. Chem*., 1961, vol. 65, pp. 581–91.
37. M.T. Nagata, J.G. Speer, and D.K. Matlock: *Metall. Mater. Trans. A*., 2002, vol. 33, pp. 3099–3110.
38. J. Kunze, C. Mickel, M. Leonhardt, and S. Oswald: *Steel. Res*., 1997, vol. 68, pp. 403–08.
39. A.M. Sage and R.C. Cochrane: The development of a weldable normalized vanadium titanium structural steel, Vanadium international technical committee, Vanitec, London, November, 1988.
40. J. Stock, C.M. Enloe, R.J. O'Malley, and K.O. Findley: *AIST Trans*., 2014, vol. 11, pp. 180–87.
41. D. Shangguan, S. Ahuja, and D.M. Stefanescu: *Metall. Trans. A*., 1992, vol. 23A, pp. 669–80.
42. M.A. Van Ende, M. Guo, E. Zinngrebe, B. Blanpain, and I.H. Jung: *ISIJ Int*., 2013, vol. 53, pp. 1974–82.
43. H.I. Aaronson, C. Laird, and K.R. Kinsman: *Phase Transformation*, ASM, Metals Park, 1970.